IEEE Access
Multidisciplinary | Rapid Review | Open Access Journal

Received January 8, 2019, accepted January 31, 2019, date of publication February 6, 2019, date of current version February 22, 2019.

Digital Object Identifier 10.1109/ACCESS.2019.2897638

In-Motion Attitude and Position Alignment for Odometer-Aided SINS Based on Backtracking Scheme

YIDING SUN, LIFEN WANG, QINGZHONG CAI, GONGLIU YANG, AND ZEYANG WEN
Instrumentation and Optoelectronic Engineering, Beihang University, Beijing 100191, China

Corresponding author: Qingzhong Cai (qingzhong_cai@163.com)

This work was supported in part by the National Natural Science Foundation of China under Grant 61803015, in part by the National Key R&D Program of China under Grant 2016YFB0501600, and in part by the National Equipment Pre-Research Foundation under Grant 6140517020101.

ABSTRACT In-motion alignment of navigation-grade strapdown inertial navigation system (SINS) combined with odometer (OD) is one of the challenging issues for the land vehicle navigation, while most current in-motion alignment methods still rely on the measurements of the global positioning system or only aim at improving the attitude alignment, thus neglecting the position alignment. Thus, one of the main obstacles during the in-motion alignment for SINS/OD is to autonomously and simultaneously obtain the high-precision attitude and position within specified time. In this paper, an in-motion alignment scheme based on the backtracking scheme is presented to solve this problem. The proposed method consists of two steps. First, an improved optimization-based coarse alignment (IOBCA) is employed to obtain the attitude and position with reasonable precision, and the gravity deflexion error projection in inertial frame caused by the positioning error is diminished, which contributes to better alignment results for the subsequent process. Second, initialized with the alignment results provided by IOBCA, a backtracking-scheme-based fine alignment combined with the Kalman filter is investigated to make a further improvement in the precision of attitude and position, during which the known initial binding position and zero velocity have been utilized again. The car-mounted field experimental results illustrate that the proposed method can not only autonomously improve the precision of attitude within a short time but also simultaneously achieve the position with high precision.

INDEX TERMS In-motion alignment, strapdown inertial navigation system (SINS), odometer (OD), backtracking.

I. INTRODUCTION

Strapdown inertial navigation system (SINS) is one of the most widely used navigation systems for positioning and attitude determination [1]. Initial alignment that determines the initial conditions prior to navigational computation is vitally important for dead-reckoning-based SINS. Due to the fact that an increasing number of land vehicles are required to complete the initial alignment in maneuvering environments, in-motion alignment has become a concern issue. Generally, external navigation sensors such as Global Positioning System (GPS) and odometer (OD), etc, are designed to provide auxiliary information for the in-motion alignment of SINS [2]–[5]. Whereas the signal of GPS is susceptible to interference and not available in jamming and masking environments especially in urban areas [6]. In contrast, OD can transform the impulses at equal angle intervals into velocity or mileage increment by multiplying the OD scale factor. Moreover, both OD and SINS have fully self-contained characteristics. Thus, OD aided SINS (SINS/OD) is expected to resist interference from surrounding environment to a great extent. In this respect, autonomous in-motion alignment designed for SINS/OD has drawn wide attention.

Normally, the initial alignment is divided into two phases, i.e., coarse alignment and fine alignment. With the roughly known initial attitude provided by coarse alignment, fine alignment can be executed under the guarantee of linear filtering model [7], [8]. Typically, utilizing the gravity

The associate editor coordinating the review of this manuscript and approving it for publication was Edith C.-H. Ngai.

observations in inertial reference frame is an effective approach to coarse alignment [9]–[14]. In [9] and [10], the TRIAD (TRIaxial Attitude Determination) algorithm which employed only three out of the four pieces of information obtainable from two measured vectors to compute an attitude solution is developed. To make sufficient utilization of the observations, Wu *et al*. [11] transformed the coarse initial alignment into an attitude determination problem using infinite vector observations over a continuous time interval, which was recognized as optimization-based coarse alignment (OBCA) method, and the recursive Davenport's q-method was developed to solve the attitude determination problem [15]. With respect to the application for external velocity aided SINS in GPS-denied scenarios, Yuan *et al*. [12] presented a novel OBCA method using the velocity loci and pressure sensor for autonomous underwater vehicles (AUV). Since the severe disturbance cannot be handled adequately by the OBCA method, Chang *et al*. [13] designed a low-pass finite impulse response digital filter to attenuate the severe disturbance inherent in the OD. In order to better compensate for the dynamic errors of gyroscope induced by severe maneuvering, Huang *et al*. [14] proposed a novel Kalman-filtering-based in-motion coarse alignment on the basis of a closed-loop approach. However, the primary concern of aforementioned discussions were to enhance the performance of attitude alignment. It is worth mentioning that position precision and speediness are also vitally important evaluation indicators during in-motion alignment. An UnScented QUaternion Estimator (USQUE)-based fine alignment method from the very start utilizing the large misalignment provided by OBCA method was developed in [16], the scheme can obtain the attitude and position simultaneously for marine application. Whereas due to the limited time determined by aforementioned scheme and marine application, the velocity measurement parameters had not been considered. Yan *et al*. [17] presented a in-motion attitude and position alignment algorithm based on inertial reference frame to diminish the gravity deflexion error for SINS/OD. On the basis of [17], Guo *et al*. [18] further excluded the negative effect of Coriolis item and utilized a optimizational attitude estimation algorithm. Though the satisfied attitude was derived, the approximately position need further improvements.

In recent few years, with the development of navigation computer technology, the backtracking navigation has been investigated to improve the navigation performance with certain length of navigation data [19]–[22]. Significant improvements in attitude performance of in-motion alignment have been achieved in [19]–[21]. In order to solve the positioning problem after the accomplishment of in-motion alignment without the aid of GPS. Li *et al*. [22] investigated a backtracking navigation scheme based on a INS error model to obtain the attitude and position. However, the speed measurement equipment errors during fine alignment were omitted. Meanwhile, initial binding position and zero velocity were only used as the initial information for dead reckoning (DR), which was considered to be underutilized. Therefore, further improvements regarding the attitude and position alignment performances of in-motion alignment would be worthwhile.

In this paper, we propose a novel in-motion alignment method, which not only autonomously improves the precision of attitude within short time but also simultaneously achieves the position with high precision. The investigated in-motion alignment method is composed of coarse alignment and fine alignment. During the process of coarse alignment, we execute the method proposed in [17] combined with an optimization-based attitude determination solution to obtain the attitude and position on the basis of the known initial information including initial binding position and zero velocity, which is defined as improved optimization-based coarse alignment (IOBCA). Then initialized with the alignment results provided by IOBCA, a backtracking-scheme-based fine alignment (BSFA) combined with Kalman filter is proposed to make a further improvement in the precision of attitude and position, during which the known initial information is utilized again. Finally, three car-mounted field tests are carried out to verify the validity and applicability of investigated method.

The remainder of this paper is organized as follows. Section II presents the reference frame definitions. Section III is devoted to the implementation of the IOBCA. In Section IV, the BSFA including backtracking SINS algorithm, backtracking dead reckoning algorithm and backtracking SINS algorithm is derived. In Section V, the proposed method and existing in-motion alignment methods are compared through three car-mounted field tests. Finally, the conclusion is drawn in Section VI.

II. THE REFERENCE FRAME DEFINITIONS

The reference coordinate frames involved in this paper are defined as follows:

i frame: Earth-Centred Initially Fixed (ECIF) orthogonal reference frame.

e frame: Earth-Centred Earth Fixed (ECEF) orthogonal reference frame.

b frame: Orthogonal reference frame aligned with Right-Forth-Up (RFU) axes.

n frame: Orthogonal reference frame aligned with actual East-North-Up (ENU) geodetic axes.

n' frame: Orthogonal reference frame aligned with computational East-North-Up (ENU) geodetic axes.

n_0 frame: Orthogonal reference frame nonrotating relative to the *e* frame. It's formed by fixing the *n* frame at the beginning of the in-motion alignment.

i_0 frame: Orthogonal reference frame nonrotating relative to the *i* frame. It's formed by fixing the *i* frame at the beginning of the in-motion alignment.

i_{b0} frame: Orthogonal reference frame nonrotating relative to the *i* frame. It's formed by fixing the *b* frame at the beginning of the in-motion alignment.

III. IMPROVED OPTIMIZATION-BASED COARSE ALIGNMENT

A. DECOMPOSITION OF THE ATTITUDE MATRIX

IOBCA starts from time t_0, the attitude matrix $\boldsymbol{C}_b^n(t)$ denotes the attitude matrix from b frame to n frame at time t, which can be decomposed into four parts as

$$\boldsymbol{C}_b^n(t) = \boldsymbol{C}_{n_0}^n(t)\boldsymbol{C}_{i_0}^{n_0}(t)\boldsymbol{C}_{i_{b0}}^{i_0}\boldsymbol{C}_b^{i_{b0}}(t) \tag{1}$$

where $\boldsymbol{C}_{n_0}^n(t)$ that encodes the attitude change of n frame is the attitude matrix from n_0 frame to n frame at time t, $\boldsymbol{C}_{i_0}^{n_0}(t)$ that encodes the attitude change of n_0 frame is the attitude matrix from i_0 frame to n_0 frame at time t. $\boldsymbol{C}_b^{i_{b0}}(t)$ that encodes the attitude change of i_{b0} frame is the attitude matrix from b frame to i_{b0} frame at time t. And $\boldsymbol{C}_{i_{b0}}^{i_0}$ is a constant attitude matrix from i_{b0} frame to i_0 frame.

At the beginning of the coarse alignment, $\boldsymbol{C}_b^{i_{b0}}(t)$ is firstly initialized as

$$\boldsymbol{C}_b^{i_{b0}}(t_0) = \boldsymbol{I}_3 \tag{2}$$

where $\boldsymbol{I}_3$ denotes the 3×3 identity matrix.

Subsequent orientation of $\boldsymbol{C}_b^{i_{b0}}(t)$ is updated by the gyroscope output $\boldsymbol{\omega}_{ib}^b = \boldsymbol{\omega}_{i_{b0}b}^b$

$$\dot{\boldsymbol{C}}_b^{i_{b0}}(t) = \boldsymbol{C}_b^{i_{b0}}(t)\left(\boldsymbol{\omega}_{ib}^b(t)\times\right) \tag{3}$$

where $(\cdot\times)$ denotes the skew symmetric matrix of $(\cdot)$.

The time-varying attitude matrix $\boldsymbol{C}_{i_0}^{n_0}(t)$ can be further decomposed into a constant matrix $\boldsymbol{C}_e^{n_0}$ and a time-varying matrix $\boldsymbol{C}_{i_0}^e(t)$. That is

$$\boldsymbol{C}_{i_0}^{n_0}(t) = \boldsymbol{C}_e^{n_0}\boldsymbol{C}_{i_0}^e(t) \tag{4}$$

where

$$\boldsymbol{C}_e^{n_0} = \begin{bmatrix} 0 & 1 & 0 \\ -\sin L_0 & 0 & \cos L_0 \\ \cos L_0 & 0 & \sin L_0 \end{bmatrix}$$

$$C_{i_0}^e(t) = \begin{bmatrix} \cos(\omega_{ie}t) & \sin(\omega_{ie}t) & 0 \\ -\sin(\omega_{ie}t) & \cos(\omega_{ie}t) & 0 \\ 0 & 0 & 1 \end{bmatrix}$$

$\boldsymbol{C}_{n_0}^n(t)$ is changing with the movement of the vehicle, which can be obtained by

$$\boldsymbol{C}_{n_0}^n(t) = \boldsymbol{C}_e^n(t)\boldsymbol{C}_{n_0}^e \tag{5}$$

where

$$\boldsymbol{C}_e^n(t) = \begin{bmatrix} -\sin\lambda & \cos\lambda & 0 \\ -\sin L\cos\lambda & -\sin L\sin\lambda & \cos L \\ \cos L\cos\lambda & \cos L\sin\lambda & \sin L \end{bmatrix},$$

$$\boldsymbol{C}_{n_0}^e = \begin{bmatrix} -\sin\lambda_0 & -\sin L_0\cos\lambda_0 & \cos L_0\cos\lambda_0 \\ \cos\lambda_0 & -\sin L_0\sin\lambda_0 & \cos L_0\sin\lambda_0 \\ 0 & \cos L_0 & \sin L_0 \end{bmatrix},$$

L_0 and λ_0 denote the initial binding geographic latitude and longitude, respectively. L and λ are calculated on the basis of L_0 and λ_0, as well as the measurements provided by SINS and OD at time t. And the explicit algorithm for L and λ will be presented in next subsection.

During the in-motion alignment, the change of latitude $\triangle L = L - L_0$ and longitude $\triangle\lambda = \lambda - \lambda_0$ can be recognized as small angles. we can further derive

$$\boldsymbol{C}_{n_0}^n(t) \approx \boldsymbol{I}_3 - \begin{bmatrix} 0 & -\triangle\lambda\sin L_0 & \triangle\lambda\cos L_0 \\ \triangle\lambda\sin L_0 & 0 & \triangle L \\ -\triangle\lambda\cos L_0 & -\triangle L & 0 \end{bmatrix} \tag{6}$$

Therefore, when the constant matrix $\boldsymbol{C}_{i_{b0}}^{i_0}$ is determined, the attitude transformation $\boldsymbol{C}_b^n(t)$ can be obtained subsequently. Typically, L and λ are replaced with L_0 and λ_0 respectively in marine application because of the short sailing distance during in-motion alignment [20]. While the travelling distance is much longer for land used application. And the omission of displacement will produce a larger error in calculating the $\boldsymbol{C}_{n_0}^n(t)$, which results in the precision loss of attitude alignment. In this respect, position alignment is equally important for coarse alignment.

B. ATTITUDE AND POSITION COARSE ALIGNMENT

The specific force equation expressed in the n frame is known as [1]

$$\dot{\boldsymbol{v}}^n(t) = \boldsymbol{C}_b^n(t)\boldsymbol{f}^b(t) - [2\boldsymbol{\omega}_{ie}^n(t) + \boldsymbol{\omega}_{en}^n(t)] \times \boldsymbol{v}^n(t) + \boldsymbol{g}^n \tag{7}$$

where $\boldsymbol{v}^n = \begin{bmatrix} v_E^n & v_N^n & v_U^n \end{bmatrix}^T$ is the velocity projected in the n frame, $\boldsymbol{f}^b$ is the specific force measured by accelerometers in the b frame, $\boldsymbol{g}^n = \begin{bmatrix} 0 & 0 & -g \end{bmatrix}^T$ is the gravity in the n frame, $\boldsymbol{\omega}_{ie}^n = \begin{bmatrix} 0 & \omega_{ie}^n\cos L & \omega_{ie}^n\sin L \end{bmatrix}^T$ denotes the earth rotation rate projected in the n frame, $\boldsymbol{\omega}_{en}^n = \begin{bmatrix} -v_N^n/(R_M + h) & v_E^n(R_N + h) & v_E^n\tan L(R_N + h) \end{bmatrix}^T$ denotes the angular rate of the n frame with respect to the e frame, R_M and R_N calculated by SINS latitude are the radius of curvature in meridian and prime vertical, respectively.

Defining $\boldsymbol{v}^{i_{b0}}$ as the velocity projected in the i_{b_0} frame. The relationship between $\boldsymbol{v}^n(t)$ and $\boldsymbol{v}^{i_{b0}}(t)$ can be expressed as

$$\begin{aligned} \dot{\boldsymbol{v}}^n(t) &= \frac{d[\boldsymbol{C}_{i_{b_0}}^n(t)\boldsymbol{v}^{i_{b0}}(t)]}{dt} \\ &= \boldsymbol{C}_{i_{b_0}}^n(t)[\dot{\boldsymbol{v}}^{i_{b0}}(t) + \boldsymbol{\omega}_{ni_{b_0}}^{i_{b_0}}(t) \times \boldsymbol{v}^{i_{b0}}(t)] \end{aligned} \tag{8}$$

where $\boldsymbol{C}_n^{i_{b0}}(t)$ that encodes the attitude change of the i_{b_0} frame is the attitude matrix from the n frame to the i_{b0} frame at time t, $\boldsymbol{\omega}_{ni_{b_0}}^{i_{b_0}}(t)$ encodes the angular rate of the i_{b_0} frame with respect to the n frame expressed in the n frame.

Substituting (8) into (7) and multiplying $\boldsymbol{C}_n^{i_{b0}}(t)$ on both side of (7), the specific force equation expressed in the i_{b0} frame is given by

$$\begin{aligned} &\dot{\boldsymbol{v}}^{i_{b0}}(t) + \boldsymbol{\omega}_{ni_{b_0}}^{i_{b_0}}(t) \times \boldsymbol{v}^{i_{b0}}(t) \\ &= \boldsymbol{C}_n^{i_{b0}}(t)\{\boldsymbol{C}_b^n(t)\boldsymbol{f}^b - [2\boldsymbol{\omega}_{ie}^n(t) + \boldsymbol{\omega}_{en}^n(t)] \times \boldsymbol{v}^n(t) + \boldsymbol{g}^n\} \end{aligned} \tag{9}$$

For any time instant t, we have

$$\boldsymbol{\omega}_{ni_{b_0}}^{i_{b_0}}(t) = -\boldsymbol{\omega}_{in}^{i_{b_0}}(t) \tag{10}$$

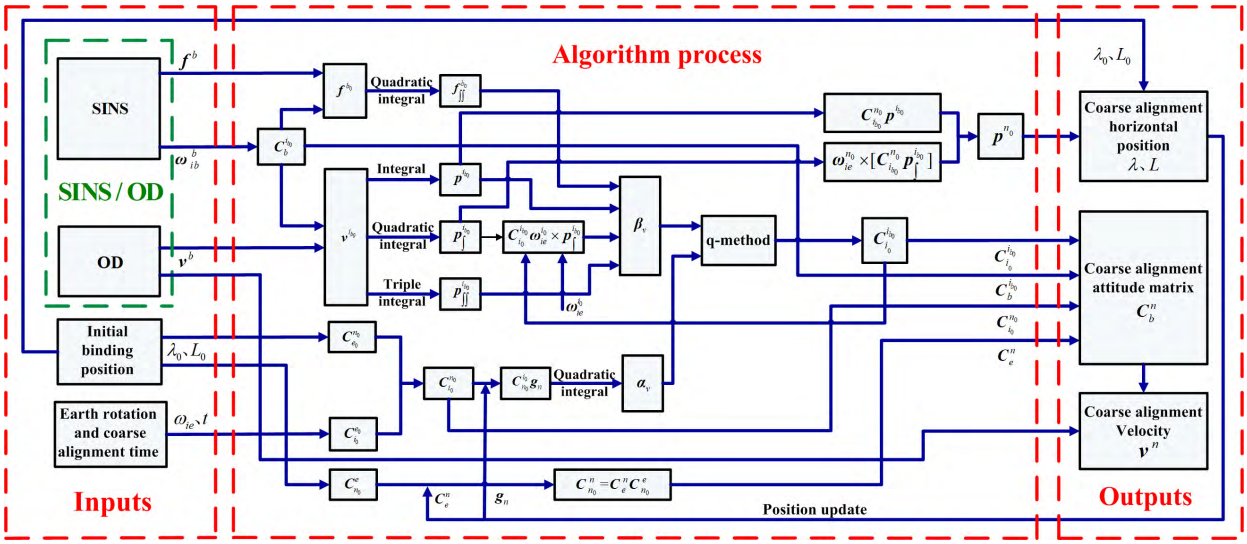

FIGURE 1. Diagram of the IOBCA for OD-aided SINS.

where $\boldsymbol{\omega}_{in}^{i_{b_0}}(t)$ encodes angular rate of the n frame with respect to the i frame expressed in the i_{b_0} frame.

Substituting (6) and (10) into (9), and then reorganizing the equation yields

$$\begin{aligned}&\dot{\boldsymbol{v}}^{i_{b_0}}(t) - \boldsymbol{C}_b^{i_{b_0}}(t)\boldsymbol{f}^b(t) + \boldsymbol{C}_{i_0}^{i_{b_0}}(t)\boldsymbol{\omega}_{ie}^{i_0}(t) \times \boldsymbol{v}^{i_{b_0}}(t)\\ &\quad = \boldsymbol{C}_n^{i_{b_0}}(t)\boldsymbol{g}^n\\ &\quad = \boldsymbol{C}_{i_0}^{i_{b_0}}\boldsymbol{C}_{n_0}^{i_0}(t)\boldsymbol{C}_n^{n_0}(t)\boldsymbol{g}^n \end{aligned} \tag{11}$$

According to (6), $\boldsymbol{C}_n^{n_0}(t)\boldsymbol{g}^n$ can be approximately expressed as

$$\boldsymbol{C}_n^{n_0}(t)\boldsymbol{g}^n \approx \boldsymbol{g}^n - g \cdot \left[\triangle\lambda \cos L_0 \ \triangle L \ 0\right]^T \tag{12}$$

The eastward and northward displacement of the vehicle can be approximated as

$$p_E^{n_0}(t) \approx R_e \triangle\lambda \cos L_0, p_N^{n_0}(t) \approx R_e \triangle L \tag{13}$$

where R_e denotes the radius of earth approximately.

Defining $\boldsymbol{p}^{n_0}(t) = \left[p_E^{n_0}(t) \ p_N^{n_0}(t) \ p_U^{n_0}(t)\right]^T$ as the displacement of the vehicle. Because the height displacement is relatively small in land used application, substituting (13) into (12) we can derive that

$$\boldsymbol{C}_n^{n_0}(t)\boldsymbol{g}^n = \boldsymbol{g}^n - \frac{g}{R_e}\left[p_E^{n_0}(t) \ p_N^{n_0}(t) \ 0\right]^T \approx \boldsymbol{g}^n - \frac{g}{R_e}\boldsymbol{p}^{n_0}(t) \tag{14}$$

Substituting (14) into (11), and then reorganizing the equation yields

$$\begin{aligned}&\dot{\boldsymbol{v}}^{i_{b_0}}(t) - \boldsymbol{C}_b^{i_{b_0}}(t)\boldsymbol{f}^b(t) + \boldsymbol{C}_{i_0}^{i_{b_0}}(t)\boldsymbol{\omega}_{ie}^{i_0}(t)\\ &\qquad \times \boldsymbol{v}^{i_{b_0}}(t) + \frac{g}{R_e} \cdot \boldsymbol{p}^{i_{b_0}}(t) = \boldsymbol{C}_{i_0}^{i_{b_0}}\boldsymbol{C}_{n_0}^{i_0}(t)\boldsymbol{g}^n \end{aligned} \tag{15}$$

where the third part on the left side of (15) is recognized as the coriolis force produced by vehicle movement and earth rotation, the forth part on the left side of (15) is recognized as the gravity deflexion produced by vehicle movement. For severe maneuvering land vehicles, the compensations of coriolis force and gravity deflexion are essential to enhance the performance of coarse alignment.

In order to attenuate the disturbance inherent in OD and improve the calculation accuracy of $\boldsymbol{C}_{i_0}^{i_{b_0}}$, double integrating (15) on both sides over the time interval of interest. The initial value of integral and quadratic integral are zero

$$\boldsymbol{\beta}_v = \boldsymbol{C}_{i_0}^{i_{b_0}}\boldsymbol{\alpha}_v \tag{16}$$

$$\boldsymbol{\alpha}_v = \int_0^t \int_0^v \boldsymbol{C}_{n_0}^{i_0}(u)\boldsymbol{g}^n du dv \tag{17}$$

$$\begin{aligned}\boldsymbol{\beta}_v = \boldsymbol{p}^{i_{b_0}}(t) &- \int_0^t \int_0^v \boldsymbol{C}_b^{i_{b_0}}(u)\boldsymbol{f}^b(u) du dv\\ &+ \boldsymbol{C}_{i_0}^{i_{b_0}}\boldsymbol{\omega}_{ie}^{i_0} \times \boldsymbol{p}_{\int}^{i_{b_0}}(t) + \frac{g}{R_e} \cdot \boldsymbol{p}_{\iint}^{i_{b_0}}(t) \end{aligned} \tag{18}$$

where

$$\begin{aligned}\boldsymbol{p}^{i_{b_0}}(t) &= \int_0^t \boldsymbol{v}^{i_{b_0}}(\tau)d\tau = \int_0^t \boldsymbol{C}_b^{i_{b_0}}(\tau)\boldsymbol{v}^b(\tau)d\tau,\\ \boldsymbol{p}_{\int}^{i_{b_0}}(t) &= \int_0^t \boldsymbol{p}^{i_{b_0}}(\tau)d\tau,\\ \boldsymbol{p}_{\iint}^{i_{b_0}}(t) &= \int_0^t \boldsymbol{p}_{\int}^{i_{b_0}}(\tau)d\tau. \end{aligned}$$

In this respect, the determination of $\boldsymbol{C}_{i_0}^{i_{b_0}}$ has been transformed into a Wahba's problem [23] with the corresponding infinite vector observations (17) and (18). Many effective approachs have been proposed for such problem. In this paper, Davenport's q method is conducted as the solution and the explicit determination procedure is presented in [15].

It should be note that the third part of $\boldsymbol{\beta}_v$ in (18) which includes the attitude matrix $\boldsymbol{C}_{i_0}^{i_{b_0}}$ is unknown when IOBCA begins. So this part is omitted to calculate the attitude matrix $\boldsymbol{C}_{i_0}^{i_{b_0}}$ approximately during short initial period. And then the attitude matrix $\boldsymbol{C}_{i_0}^{i_{b_0}}$ can be obtain with no omition in $\boldsymbol{\alpha}_v$ by utilizing the approximate $\boldsymbol{C}_{i_0}^{i_{b_0}}$. In addition, since the (17)

and (18) have declared that the initial value of integral is zero, the $\boldsymbol{v}^b(t)$ in $\boldsymbol{p}^{i_{b_0}}(t)$ should be initialized with zero. That is, the car is expect to remain stationary when IOBCA begins execution.

In order to obtain the attitude matrix $\boldsymbol{C}_{n_0}^{n}(t)$ with rational precision, the calculation of the $\boldsymbol{p}^{n_0}(t)$, which determines the $\triangle L$ and $\triangle\lambda$, is considered to be an essential issue. According to the integration by parts, we can derive that

$$\begin{aligned}\boldsymbol{p}^{n_0}(t) &= \int_0^t \dot{\boldsymbol{v}}^{n_0}(\tau)d\tau \\ &= \int_0^t \boldsymbol{C}_{i_{b_0}}^{n_0}(\tau)\dot{\boldsymbol{p}}^{i_{b_0}}(\tau)d\tau \\ &= \boldsymbol{C}_{i_{b_0}}^{n_0}(t)\boldsymbol{p}^{i_{b_0}}(t) - \int_0^t \boldsymbol{\omega}_{n_0 i_{b_0}}^{n_0}(\tau)\times[\boldsymbol{C}_{i_{b_0}}^{n_0}(\tau)\boldsymbol{p}^{i_{b_0}}(\tau)]d\tau\end{aligned} \tag{19}$$

where $\boldsymbol{C}_{i_{b_0}}^{n_0}(t) = \boldsymbol{C}_{i_0}^{n_0}(t)\boldsymbol{C}_{i_{b_0}}^{i_0}$ that encodes the attitude change of the n_0 frame is the attitude matrix from the i_{b_0} frame to the n_0 frame at time t, $\boldsymbol{\omega}_{n_0 i_{b_0}}^{n_0}(t)$ encodes the angular rate from i_{b_0} frame with respect to n_0 frame expressed in the n_0 frame.

As the earth rotation is relatively small and coarse alignment time is short, thus $\omega_{ie}t$ in $\boldsymbol{C}_{i_0}^{e_0}(t)$ is a small angle, i.e. $\boldsymbol{C}_{i_0}^{e_0}(t) \approx \boldsymbol{I}_3$. In this respect, $\boldsymbol{C}_{i_{b_0}}^{n_0}(t)$ is recognized as a constant attitude matrix approximately at time t_0, Thus we can derive that

$$\boldsymbol{C}_{i_{b_0}}^{n_0}(t) = \boldsymbol{C}_{e_0}^{n_0}\boldsymbol{C}_{i_0}^{e_0}(t)\boldsymbol{C}_{i_{b_0}}^{i_0} \approx \boldsymbol{C}_{i_{b_0}}^{n_0}(t_0) \tag{20}$$

For any time instant t, we have

$$\boldsymbol{\omega}_{n_0 i_{b_0}}^{n_0}(t) = -\boldsymbol{\omega}_{ie}^{n_0} \tag{21}$$

Substituting (20) and (21) into (19), $\boldsymbol{p}^{n_0}(t)$ can be calculated by

$$\boldsymbol{p}^{n_0}(t) = \boldsymbol{C}_{i_{b_0}}^{n_0}(t)\boldsymbol{p}^{i_{b_0}}(t) + \boldsymbol{\omega}_{ie}^{n_0}\times[\boldsymbol{C}_{i_{b_0}}^{n_0}(t_0)\boldsymbol{p}_{\int}^{i_{b_0}}(t)] \tag{22}$$

And then the λ and L can be calculated by

$$\lambda = \lambda_0 + \frac{p_E^{n_0}(t)}{(R_N+h_0)\cos L_0} \tag{23a}$$

$$L = L_0 + \frac{p_N^{n_0}(t)}{R_M+h_0} \tag{23b}$$

Therefore, the real-time attitude which determined by the attitude matrix $\boldsymbol{C}_b^n$ and the real-time horizontal position L and λ can be obtained during the coarse alignment. In the meantime, the real-time velocity $\boldsymbol{v}^n$ can be obtained by

$$\boldsymbol{v}^n = \boldsymbol{C}_b^n\boldsymbol{v}^b \tag{24}$$

where $\boldsymbol{v}^b$ is the velocity measured by OD expressed in the b frame. The diagram of IOBCA for OD-aided SINS is shown in Fig. 1, which illustrates the essential inputs, algorithms process and real-time outputs of IOBCA. In this respect, the attitude, velocity and position provided by IOBCA at the end of coarse alignment can be set as the initialization parameters of fine alignment. And the explicit process of fine alignment is presented in next section.

IV. BACKTRACKING-SCHEME-BASED FINE ALIGNMENT

A. BACKTRACKING SINS ALGORITHM

The backtracking SINS algorithm is based on the forward SINS algorithm, so the latter is introduced firstly. The forward SINS algorithm is consisted of three parts: attitude navigation algorithm, velocity navigation algorithm and position navigation algorithm, which can be written as three first-order differential equations

$$\dot{\boldsymbol{C}}_b^n = \boldsymbol{C}_b^n\boldsymbol{\Omega}_{nb}^b \tag{25a}$$

$$\dot{\boldsymbol{v}}^n(t) = \boldsymbol{C}_b^n(t)\boldsymbol{f}^b(t) - [2\boldsymbol{\omega}_{ie}^n(t)+\boldsymbol{\omega}_{en}^n(t)]\times\boldsymbol{v}^n(t)+\boldsymbol{g}^n \tag{25b}$$

$$\dot{L} = v_N^n(R_M+h), \quad \dot{\lambda} = v_E^n\sec L/(R_N+h), \ \dot{h} = v_U^n \tag{25c}$$

where

$$\boldsymbol{\Omega}_{nb}^b = (\boldsymbol{\omega}_{nb}^b\times), \quad \boldsymbol{\omega}_{nb}^b = \boldsymbol{\omega}_{ib}^b - (\boldsymbol{C}_b^n)^T(\boldsymbol{\omega}_{ie}^n + \boldsymbol{\omega}_{en}^n).$$

In practice, in order to perform the recursion calculation in a computer, the forward SINS algorithm in (24) should be discretized

$$\boldsymbol{C}_{bk}^n = \boldsymbol{C}_{bk-1}^n(\boldsymbol{I}_3 + T_s\boldsymbol{\Omega}_{nbk}^b) \tag{26a}$$

$$\begin{aligned}\boldsymbol{v}_k^n = \boldsymbol{v}_{k-1}^n &+ T_s[\boldsymbol{C}_{bk-1}^n\boldsymbol{f}_k^b \\ &- (2\boldsymbol{\omega}_{iek-1}^n + \boldsymbol{\omega}_{enk-1}^n)\times\boldsymbol{v}_{k-1}^n + \boldsymbol{g}^n]\end{aligned} \tag{26b}$$

$$\begin{aligned}L_k &= L_{k-1} + T_s v_{Nk-1}^n/(R_N+h_{k-1}) \\ \lambda_k &= \lambda_{k-1} + T_s v_{Ek-1}^n\sec L_{k-1}/(R_N+h_{k-1}) \\ h_k &= h_{k-1} + T_s v_{Uk-1}^n\end{aligned} \tag{26c}$$

where

$$\begin{aligned}\boldsymbol{\Omega}_{nbk}^b &= (\boldsymbol{\omega}_{nbk}^b\times), \quad \boldsymbol{\omega}_{nbk}^b \\ &= \boldsymbol{\omega}_{ibk}^b - (\boldsymbol{C}_{bk-1}^n)^T(\boldsymbol{\omega}_{iek-1}^n + \boldsymbol{\omega}_{enk-1}^n), \\ \boldsymbol{\omega}_{iek}^n &= [0\ \omega_{ie}^n\cos L_k\ \omega_{ie}^n\sin L_k]^T, \\ \omega_{enk}^n &= \begin{bmatrix} -v_{Nk}^n/(R_M+h_k) \\ v_{Ek}^n/(R_N+h_k) \\ v_{Ek}^n\tan L_k/(R_N+h_k)\end{bmatrix}.\end{aligned}$$

T_s is the sampling time of gyroscopes and accelerometers in SINS, k is each discretized time point of the navigation process (k = 1,2,3,. . .).

Assuming that SINS navigates from position A to position B from time t_0 to t, the backtracking discreted SINS algorithm from position B back to position A is that [24]

$$\begin{aligned}\boldsymbol{C}_{bk-1}^n &= \boldsymbol{C}_{bk}^n(\boldsymbol{I}_3 + T_s\boldsymbol{\Omega}_{nbk}^b)^{-1} \\ &\approx \boldsymbol{C}_{bk}^n(\boldsymbol{I}_3 - T_s\boldsymbol{\Omega}_{nbk}^b) \\ &\approx \boldsymbol{C}_{bk}^n(\boldsymbol{I}_3 + T_s\widetilde{\boldsymbol{\Omega}}_{nbk-1}^b)\end{aligned} \tag{27a}$$

$$\begin{aligned}\boldsymbol{v}_{k-1}^n &= \boldsymbol{v}_k^n - T_s[\boldsymbol{C}_{bk-1}^n\boldsymbol{f}_k^b \\ &\quad - (2\boldsymbol{\omega}_{iek-1}^n + \boldsymbol{\omega}_{enk-1}^n)\times\boldsymbol{v}_{k-1}^n + \boldsymbol{g}^n] \\ &\approx \boldsymbol{v}_k^n - T_s[\boldsymbol{C}_{bk}^n\boldsymbol{f}_{k-1}^b \\ &\quad - (2\boldsymbol{\omega}_{iek}^n + \boldsymbol{\omega}_{enk}^n)\times\boldsymbol{v}_k^n + \boldsymbol{g}^n]\end{aligned} \tag{27b}$$

$$\begin{aligned} L_{k-1} &= L_k - T_s v^n_{Nk-1}/(R_M + h_{k-1}) \\ &\approx L_k - T_s v^n_{Nk}/(R_M + h_k) \\ \lambda_{k-1} &= \lambda_k - T_s v^n_{Ek-1} \sec L_{k-1}/(R_N + h_{k-1}) \\ &\approx \lambda_k - T_s v^n_{Ek} \sec L_k/(R_N + h_k) \\ h_{k-1} &= h_k - T_s v^n_{Uk-1} \approx h_k - T_s v^n_{Uk} \end{aligned} \tag{27c}$$

where

$$\begin{aligned} \widetilde{\boldsymbol{\Omega}}^b_{nbk-1} &= (\widetilde{\boldsymbol{\omega}}^b_{nbk-1}\times), \quad \widetilde{\boldsymbol{\omega}}^b_{nbk-1} \\ &= -[\boldsymbol{\omega}^b_{ibk-1} - (\boldsymbol{C}^n_{bk})^T(\boldsymbol{\omega}^n_{iek} + \boldsymbol{\omega}^n_{enk})]. \end{aligned}$$

It can be seen that the backtracking discreted SINS algorithm is similar to the forward discreted SINS algorithm except that the sign of initial velocity, gyroscope measurements and earth rotation are opposite. Defining the $\boldsymbol{v}^n_{Bk} = -\boldsymbol{v}^n_k$ as the backtracking SINS velocity, the backtracking SINS algorithm can be rewritten as

$$\boldsymbol{C}^n_{bk-1} \approx \boldsymbol{C}^n_{bk}(\boldsymbol{I}_3 + T_s\widetilde{\boldsymbol{\Omega}}^b_{nbBk-1}) \tag{28a}$$

$$\begin{aligned} \boldsymbol{v}^n_{Bk-1} \approx \boldsymbol{v}^n_{Bk} + T_s[&\boldsymbol{C}^n_{bk}\boldsymbol{f}^b_{k-1} \\ &-(-2\boldsymbol{\omega}^n_{iek} + \boldsymbol{\omega}^n_{enBk})\times \boldsymbol{v}^n_{Bk} + \boldsymbol{g}^n] \end{aligned} \tag{28b}$$

$$\begin{aligned} L_{k-1} &\approx L_k + T_s v^n_{NBk}/(R_M + h_k) \\ \lambda_{k-1} &\approx \lambda_k + T_s v^n_{EBk} \sec L_k/(R_N + h_k) \\ h_{k-1} &\approx h_k + T_s v^n_{UBk} \end{aligned} \tag{28c}$$

where

$$\begin{aligned} \widetilde{\boldsymbol{\Omega}}^b_{nbBk-1} &= (\widetilde{\boldsymbol{\omega}}^b_{nbBk-1}\times), \\ \widetilde{\boldsymbol{\omega}}^b_{nbBk-1} &= -\boldsymbol{\omega}^b_{ibk-1} - (\boldsymbol{C}^n_{bk})^T(\boldsymbol{\omega}^n_{iek} + \boldsymbol{\omega}^n_{enBk}), \\ \omega^n_{enBk} &= \begin{bmatrix} -v^n_{NBk}/(R_M + h_k) \\ v^n_{EBk}/(R_N + h_k) \\ v^n_{EBk}\tan L_k/(R_N + h_k) \end{bmatrix}. \end{aligned}$$

B. BACKTRACKING DEAD RECKONING ALGORITHM

SINS/OD can be recognized as a DR system, assuming that the sampling time of OD is T_s as well. Thus $\boldsymbol{v}^b_{sk}$ which encodes the velocity measured by OD expressed in the b frame at time t_k can be calculated by

$$\boldsymbol{v}^b_{sk} = \triangle \boldsymbol{s}^b_k/T_s \tag{29}$$

where $\triangle \boldsymbol{s}^b_k$ encodes the mileage increment expressed in the b frame at time t_k.

With the auxiliary velocity measurements provided by OD, the discreted forward DR algorithm can be derived that

$$\boldsymbol{C}^n_{bk} = \boldsymbol{C}^n_{bk-1}(\boldsymbol{I}_3 + T_s\boldsymbol{\Omega}^b_{nbk}) \tag{30a}$$

$$\begin{aligned} \boldsymbol{v}^n_{sk} &= \boldsymbol{C}^n_{bk-1}\boldsymbol{v}^b_{sk} \\ L_{Dk} &= L_{Dk-1} + T_s v^n_{sNk-1}/(R_{DM} + h_{Dk-1}) \\ \lambda_{Dk} &= \lambda_{Dk-1} + T_s v^n_{sEk-1} \sec L_{Dk-1}/(R_{DN} + h_{Dk-1}) \\ h_{Dk} &= h_{Dk-1} + T_s v^n_{sUk-1} \end{aligned} \tag{30b}$$

$$\tag{30c}$$

where the velocity in $\boldsymbol{\Omega}^b_{nbk}$ is required to be replaced with $\boldsymbol{v}^b_{sk}$, L_{Dk}, λ_{Dk} and h_{Dk} denote the latitude, longitude and height calculated by DR at time t_k, respectively, R_{MD} and R_{ND} calculated by DR latitude are the radius of curvature in meridian and prime vertical, respectively.

Similarly, defining the $\boldsymbol{v}^n_{sBk} = -\boldsymbol{v}^n_{sk}$ as the backtracking DR velocity, the sign of OD measurements, gyroscope measurements and earth rotation are opposite in discreted backtracking DR algorithm. The discreted backtracking DR algorithm can be written as

$$\boldsymbol{C}^n_{bk-1} \approx \boldsymbol{C}^n_{bk}(\boldsymbol{I}_3 + T_s\widetilde{\boldsymbol{\Omega}}^b_{nbBk-1}) \tag{31a}$$

$$\begin{aligned} \boldsymbol{v}^n_{sBk-1} &= \boldsymbol{C}^n_{bk}\boldsymbol{v}^b_{sBk-1} \\ L_{Dk-1} &\approx L_{Dk} + T_s v^n_{sNBk}/(R_{DM} + h_{Dk}) \\ \lambda_{Dk-1} &\approx \lambda_{Dk} + T_s v^n_{sEBk} \sec L_{Dk}/(R_{DN} + h_{Dk}) \end{aligned} \tag{31b}$$

$$h_{Dk-1} \approx h_{Dk} + T_s v^n_{sUBk} \tag{31c}$$

C. KALMAN-FITERING-BASED FINE ALIGNMENT

According to the forward SINS algorithm and forward DR algorithm, the error model of the SINS/OD can be written as [25], [26]

$$\dot{\boldsymbol{\phi}} = -\boldsymbol{\omega}^n_{in}\times\boldsymbol{\phi} + \boldsymbol{M}_{av}\delta\boldsymbol{v} + \boldsymbol{M}_{ap}\delta\boldsymbol{p} - \boldsymbol{C}^n_b\boldsymbol{\varepsilon}^b \tag{32a}$$

$$\delta\dot{\boldsymbol{v}}^n = \boldsymbol{f}^n\times\boldsymbol{\phi} + \boldsymbol{M}_{vv}\delta\boldsymbol{v} + \boldsymbol{M}_{vp}\delta\boldsymbol{p} + \boldsymbol{C}^n_b\nabla^b \tag{32b}$$

$$\delta\dot{\boldsymbol{p}} = \boldsymbol{M}_{pv}\delta\boldsymbol{v}^n + \boldsymbol{M}_{pp}\delta\boldsymbol{p} \tag{32c}$$

$$\delta\dot{\boldsymbol{p}}_D = \boldsymbol{M}_{pv}\boldsymbol{v}^n\times\boldsymbol{\phi} + \boldsymbol{M}_{pp}\delta\boldsymbol{p}_D + \boldsymbol{M}_\beta\boldsymbol{\beta} + \boldsymbol{M}_K\delta K_D \tag{32d}$$

$$\dot{\boldsymbol{\varepsilon}}^b = [0\ 0\ 0]^T \tag{32e}$$

$$\dot{\nabla}^b = [0\ 0\ 0]^T \tag{32f}$$

$$\delta\dot{K}_d = 0 \tag{32g}$$

$$\delta\dot{\boldsymbol{\beta}} = [0\ 0]^T \tag{32h}$$

where

$$\boldsymbol{M}_1 = \begin{bmatrix} 0 & 0\ 0 \\ -\omega_{ie}\sin L & 0\ 0 \\ \omega_{ie}\cos L & 0\ 0 \end{bmatrix}, \quad \boldsymbol{M}_2 = \begin{bmatrix} 0 & -\frac{1}{R_M+h} & 0 \\ \frac{1}{R_N+h} & 0 & 0 \\ \frac{\tan L}{R_N+h} & 0 & 0 \end{bmatrix},$$

$$\boldsymbol{M}_3 = \begin{bmatrix} 0 & 0 & \frac{v_N}{(R_N+h)^2} \\ 0 & 0 & -\frac{v_E}{(R_N+h)^2} \\ \frac{v_E\sec^2 L}{R_N+h} & 0 & -\frac{v_E\tan L}{(R_N+h)^2} \end{bmatrix},$$

$$\boldsymbol{M}_{av} = \boldsymbol{M}_2, \quad \boldsymbol{M}_{ap} = \boldsymbol{M}_1 + \boldsymbol{M}_3,$$

$$\boldsymbol{M}_{vv} = -\left[(\boldsymbol{v}^n\times)\boldsymbol{M}_{av} + (2\boldsymbol{\omega}^n_{ie} + \boldsymbol{\omega}^n_{en})\times\right],$$

$$\boldsymbol{M}_{vp} = (\boldsymbol{v}^n\times)(2\boldsymbol{M}_1 + \boldsymbol{M}_3),$$

$$\boldsymbol{M}_{pv} = \begin{bmatrix} 0 & \frac{1}{R_M+h} & 0 \\ \frac{\sec L}{R_N+h} & 0 & 0 \\ 0 & 0 & 1 \end{bmatrix},$$

$$\boldsymbol{M}_{pp} = \begin{bmatrix} 0 & 0 & -\frac{v_N}{(R_N+h)^2} \\ \frac{v_E\sec L\tan L}{R_N+h} & 0 & -\frac{v_E\sec L}{(R_N+h)^2} \\ 0 & 0 & 0 \end{bmatrix},$$

$$\boldsymbol{M}_\alpha = \left[-\boldsymbol{C}^n_b(:,3)\ \boldsymbol{C}^n_b(:,1)\right]v_D,$$

$$\boldsymbol{M}_{\beta} = \boldsymbol{M}_{pv}\boldsymbol{M}_{\alpha},$$
$$\boldsymbol{M}_{K} = \boldsymbol{M}_{pv}\boldsymbol{v}^{n}.$$

$\boldsymbol{\phi} = \begin{bmatrix}\phi_E & \phi_N & \phi_U\end{bmatrix}^T$, $\delta\boldsymbol{v}^n = \begin{bmatrix}\delta v_E & \delta v_N & \delta v_U\end{bmatrix}^T$, $\delta\boldsymbol{p} = \begin{bmatrix}\delta L & \delta\lambda & \delta h\end{bmatrix}^T$ and $\delta\boldsymbol{p}_D = \begin{bmatrix}\delta L_D & \delta\lambda_D & \delta h_D\end{bmatrix}^T$ are the misalignment angle vector, SINS velocity error vector, SINS position error vector and DR position error vector, respectively; $\boldsymbol{\varepsilon}^b = \begin{bmatrix}\varepsilon_x^b & \varepsilon_y^b & \varepsilon_z^b\end{bmatrix}^T$ and $\nabla^b = \begin{bmatrix}\nabla_x^b & \nabla_y^b & \nabla_z^b\end{bmatrix}^T$ are the gyroscope drift vector and accelerometer bias vector in the b frame, respectively; $\boldsymbol{\beta} = \begin{bmatrix}\delta\alpha_\theta & \delta\alpha_\varphi\end{bmatrix}^T$ is the OD installation angle error vector, in which $\delta\alpha_\theta$ denotes as the pitch installation error of OD and $\delta\alpha_\varphi$ denotes the heading installation error of OD; δK_D denotes the OD scale factor error; v_D denotes the forward velocity measured by OD.

Based on the linear state-space model given by (32), Kalman-filtering-based fine alignment is employed to estimate attitude errors and position errors. Thus, the fine alignment filter should be designed first. It should be noted that $\delta\alpha_\theta$ mainly induces the altitude error and has marginal impact on the horizontal position. Meanwhile, the altitude error and vertical velocity can be restrained by barometer altimeter. Therefore, in order to reduce the computational load, we establish the state vector $\boldsymbol{X}$ without regard to the δv_U^n, δh, ∇_z^b, δh_D and $\delta\alpha_\theta$, that is

$$\boldsymbol{X} = [\delta\phi_E\ \delta\phi_N\ \delta\phi_U\ \delta v_E\ \delta v_N\ \delta L\ \delta\lambda\ \varepsilon_x^b\varepsilon_y^b \varepsilon_z^b\ \nabla_x^b\ \nabla_y^b\ \delta L_D\ \delta\lambda_D\ \delta\alpha_\varphi\ \delta K_D]^T \quad (33)$$

During fine alignment process, attitude errors could not be acquired without external attitude reference. While under moving base, the position errors can be acquired by deducting the DR position $\tilde{\boldsymbol{p}}_D$ from the SINS position $\tilde{\boldsymbol{p}}$. Thus, the measurement variables are chosen as position errors

$$\begin{aligned}\boldsymbol{Z} &= \tilde{\boldsymbol{p}} - \tilde{\boldsymbol{p}}_D = (\boldsymbol{p}_{real} + \delta\boldsymbol{p}) - (\boldsymbol{p}_{real} + \delta\boldsymbol{p}_D)\\ &= \delta\boldsymbol{p} - \delta\boldsymbol{p}_D\end{aligned} \quad (34)$$

where $\boldsymbol{p}_{real}$ is the actual position.

Therefore, based on the (32)–(34), which denotes as the dynamic model, statement vector and measurement, respectively, the continuous 16-dimensional (16D) forward Kalman filter of fine alignment is designed as follows

$$\dot{\boldsymbol{X}} = \boldsymbol{F}\boldsymbol{X} + \boldsymbol{G}\boldsymbol{w} \quad (35a)$$
$$\boldsymbol{Z} = \boldsymbol{H}\boldsymbol{X} + \boldsymbol{v} \quad (35b)$$

where $\boldsymbol{F}$ is the state matrix; $\boldsymbol{G}$ is the noise matrix; $\boldsymbol{w}$ is the white system process noise with the power spectral density $\boldsymbol{Q}$. $\boldsymbol{H}$ is the measurement matrix. According to the (32), the expression of state matrix $\boldsymbol{F}$ is shown at the top of this page. The noise matrix $\boldsymbol{G}$ and the measurement matrix $\boldsymbol{H}$ can be expressed as follows

$$\boldsymbol{G} = \begin{bmatrix}-\boldsymbol{C}_b^n & \boldsymbol{0}_{3\times2}\\ \boldsymbol{0}_{2\times3} & \boldsymbol{C}_b^n(1:2,1:2)\\ \boldsymbol{0}_{11\times3} & \boldsymbol{0}_{11\times2}\end{bmatrix},$$
$$\boldsymbol{H} = \begin{bmatrix}\boldsymbol{0}_{2\times5} & \boldsymbol{I}_{2\times2} & \boldsymbol{0}_{2\times5} & -\boldsymbol{I}_{2\times2} & \boldsymbol{0}_{2\times2}\end{bmatrix}.$$

Based on the continuous 16D forward Kalman filter, the discretization form of 16D forward Kalman filter is given as follows

$$\boldsymbol{X}_k = \boldsymbol{\Phi}_{k-1,k}\boldsymbol{X}_{k-1} + \boldsymbol{\Gamma}_{k-1}\boldsymbol{W}_{k-1} \quad (36a)$$
$$\boldsymbol{Z}_k = \boldsymbol{H}_k\boldsymbol{X}_k + \boldsymbol{V}_k \quad (36b)$$

where $\boldsymbol{X}_k$ is the state vector at time t_k; $\boldsymbol{\Phi}_{k-1,k} = \boldsymbol{I} + T_{kf}\boldsymbol{F}(t_{k-1})$ is the state transition matrix from time t_{k-1} to t_k; T_{kf} is the Kalman filter period; $\boldsymbol{F}(t_{k-1})$ is the expression of $\boldsymbol{F}$ at time t_{k-1}; $\boldsymbol{\Gamma}_{k-1}$ is the system noise drive matrix at time t_{k-1}; $\boldsymbol{W}_{k-1}$ is the system excitation noise at time t_{k-1}, and these conditions are satisfied: $E[\boldsymbol{W}_k] = 0$, $Cov[\boldsymbol{W}_k, \boldsymbol{W}_j] = E[\boldsymbol{W}_k\boldsymbol{W}_j^T] = \boldsymbol{Q}_k\boldsymbol{\delta}_{k,j}$; $\boldsymbol{Q}_k$ is the non-negative definite variance matrix of $\boldsymbol{W}_k$; $E[\boldsymbol{V}_k] = 0$, $Cov[\boldsymbol{V}_k, \boldsymbol{V}_j] = E[\boldsymbol{V}_k\boldsymbol{V}_j^T] = \boldsymbol{R}_k\boldsymbol{\delta}_{k,j}$; $\boldsymbol{R}_k$ is the non-negative definite variance matrix of $\boldsymbol{V}_k$.

Forward Kalman filter process is organized as follows One step prediction of state

$$\hat{\boldsymbol{X}}_{k,k-1} = \boldsymbol{\Phi}_{k,k-1}\hat{\boldsymbol{X}}_{k-1} \quad (37)$$

State estimation

$$\hat{\boldsymbol{X}}_k = \hat{\boldsymbol{X}}_{k,k-1} + \boldsymbol{K}_k(\boldsymbol{Z}_k - \boldsymbol{H}_k\hat{\boldsymbol{X}}_{k,k-1}) \quad (38)$$

Gain matrix

$$\boldsymbol{K}_k = \boldsymbol{P}_{k,k-1}\boldsymbol{H}_k^T\left(\boldsymbol{H}_k\boldsymbol{P}_{k,k-1}\boldsymbol{H}_k^T + \boldsymbol{R}_k\right)^{-1} \quad (39)$$

One step prediction of mean square error

$$\boldsymbol{P}_{k,k-1} = \boldsymbol{\Phi}_{k,k-1}\boldsymbol{P}_{k-1}\boldsymbol{\Phi}_{k,k-1}^T + \boldsymbol{\Gamma}_{k-1}\boldsymbol{Q}_{k-1}\boldsymbol{\Gamma}_{k-1}^T \quad (40)$$

Mean square error estimation

$$\boldsymbol{P}_k = (\boldsymbol{I} - \boldsymbol{K}_k\boldsymbol{H}_k)\boldsymbol{P}_{k,k-1} \quad (41)$$

The backtracking Kalman filter process can be obtained by modifying the forward Kalman filter process. The statement vector and measurement of backtracking Kalman filter are same with forward Kalman filter, which are set as (33) and (34), respectively. The dynamic model of backtracking Kalman filter is much the same as the forward one except that the sign of the gyroscope measurements, the gyroscope biases and the earth rotation angular velocity in the (32) are opposite. As for the time backtracking management, it requires that the system state update to be performed in the reverse order. In one step prediction equation and state estimation, the backtracking update process is performed from $\hat{\boldsymbol{X}}_k$ to $\hat{\boldsymbol{X}}_{k-1}$, transfer matrix $\boldsymbol{\Phi}_{k,k-1}$ changes to $\boldsymbol{\Phi}_{k-1,k}$. In the one-step prediction of the mean square error equation, the prediction process is from $\boldsymbol{P}_k$ to $\boldsymbol{P}_{k-1}$. So the 16D backtracking Kalman filter process is organized as follows One step prediction of state

$$\hat{\boldsymbol{X}}_{k-1,k} = \boldsymbol{\Phi}_{k-1,k}\hat{\boldsymbol{X}}_k \quad (42)$$

State estimation

$$\hat{\boldsymbol{X}}_{k-1} = \hat{\boldsymbol{X}}_{k-1,k} + \boldsymbol{K}_{k-1}(\boldsymbol{Z}_{k-1} - \boldsymbol{H}_{k-1}\hat{\boldsymbol{X}}_{k-1,k}) \quad (43)$$

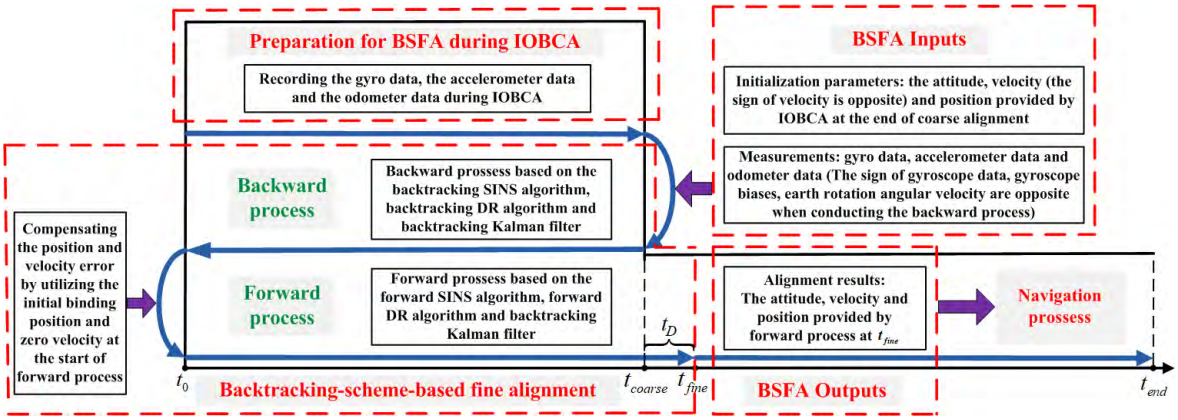

FIGURE 2. Diagram of the BSFA for OD-aided SINS.

Gain matrix

$$\boldsymbol{K}_{k-1} = \boldsymbol{P}_{k-1,k}\boldsymbol{H}_{k-1}^T \left(\boldsymbol{H}_{k-1}\boldsymbol{P}_{k-1,k}\boldsymbol{H}_{k-1}^T + \boldsymbol{R}_{k-1}\right)^{-1} \tag{44}$$

One step prediction of mean square error

$$\boldsymbol{P}_{k-1,k} = \boldsymbol{\Phi}_{k-1,k}\boldsymbol{P}_k\boldsymbol{\Phi}_{k-1,k}^T + \boldsymbol{\Gamma}_k\boldsymbol{Q}_k\boldsymbol{\Gamma}_k^T \tag{45}$$

Mean square error estimation

$$\boldsymbol{P}_{k-1} = (\boldsymbol{I} - \boldsymbol{K}_{k-1}\boldsymbol{H}_{k-1})\boldsymbol{P}_{k-1,k} \tag{46}$$

According to (37)–(46), we can estimate the attitude error and position error by employing backtracking Kalman filter and forward Kalman filter within a certain time period. It should be noted that no matter how powerful the navigation computer is, the backward process and the forward process still need time to carry out. In this respect, inevitable time delay t_D will exist during the implementation of forward process at t_{coarse}. So extra memory is essential to record the measurement information. Then the forward process will be end at t_{fine} and follow by the navigation process. It should be pointed out that the delay time t_D is very short due to the enormous computing power of modern navigation computer. Therefore, the investigated in-motion alignment method can provide high-precision attitude and position within short time all the same.

Given the above, the diagram of BSFA for OD-aided SINS is shown in Fig. 2, and the specific algorithm procedure of BSFA are summarized in the following.

1) First, IOBCA is developed to derive the attitude, velocity and position with rational precision. In the meantime, the gyro data, the accelerometer data and the OD data are recorded during IOBCA.
2) Second, the backward process of BSFA is executed. The navigational initialization parameters including the attitude, velocity (the sign is opposite) and position are provided by IOBCA at the end of coarse alignment. The specific initial backward Kalman filter parameters are introduced in Table 2. Meanwhile, the signs of gyroscope measurements, gyroscope biases, earth rotation angular velocity are opposite according to the backtracking algorithm.
3) Third, the forward process of BSFA is carried out subsequently, during which the signs of gyroscope measurements, gyroscope biases, earth rotation angular velocity return to normal. And the known initial binding position and the velocity which is zero are utilized again at the start of forward process, aiming to further refine the velocity and position estimation. In addition, all the forward Kalman filter parameters are initialized with the parameters provided by backward Kalman filter at the end of backward process. Furthermore, the convergent OD errors estimated by Kalman filter are compensated to obtain the velocity and position with higher precision.
4) Finally, initialized with the attitude, velocity and position provided by forward process, the navigation process of SINS/OD can be conducted consecutively.

$$\boldsymbol{F} = \begin{bmatrix} -\left(\boldsymbol{\omega}_{in}^n\times\right) & \boldsymbol{M}_{av}(:,1:2) & \boldsymbol{M}_{ap}(:,1:2) & -\boldsymbol{C}_b^n & \boldsymbol{0}_{3\times2} & \boldsymbol{0}_{3\times2} & \boldsymbol{0}_{3\times1} & \boldsymbol{0}_{3\times1} \\ \left(\boldsymbol{f}_{in}^n\times\right)(1:2,:) & \boldsymbol{M}_{vv}(1:2,1:2) & \boldsymbol{M}_{vp}(1:2,1:2) & \boldsymbol{0}_{2\times3} & \boldsymbol{C}_b^n(1:2,1:2) & \boldsymbol{0}_{2\times2} & \boldsymbol{0}_{2\times1} & \boldsymbol{0}_{2\times1} \\ \boldsymbol{0}_{2\times3} & \boldsymbol{M}_{pv}(1:2,1:2) & \boldsymbol{M}_{pp}(1:2,1:2) & \boldsymbol{0}_{2\times3} & \boldsymbol{0}_{2\times2} & \boldsymbol{0}_{2\times2} & \boldsymbol{0}_{2\times1} & \boldsymbol{0}_{2\times1} \\ \boldsymbol{0}_{3\times3} & \boldsymbol{0}_{3\times2} & \boldsymbol{0}_{3\times2} & \boldsymbol{0}_{3\times3} & \boldsymbol{0}_{3\times2} & \boldsymbol{0}_{3\times2} & \boldsymbol{0}_{3\times1} & \boldsymbol{0}_{3\times1} \\ \boldsymbol{0}_{2\times3} & \boldsymbol{0}_{2\times2} & \boldsymbol{0}_{2\times2} & \boldsymbol{0}_{2\times3} & \boldsymbol{0}_{2\times2} & \boldsymbol{0}_{3\times2} & \boldsymbol{0}_{3\times1} & \boldsymbol{0}_{3\times1} \\ \left[\boldsymbol{M}_{pp}(\boldsymbol{v}_D^n\times)\right](1:2,:) & \boldsymbol{0}_{2\times2} & \boldsymbol{0}_{2\times2} & \boldsymbol{0}_{2\times3} & \boldsymbol{0}_{2\times2} & \boldsymbol{M}_{pp}(1:2,1:2) & \boldsymbol{M}_{\beta}(1:2,:) & \boldsymbol{M}_K(1:2,:) \\ \boldsymbol{0}_{1\times3} & \boldsymbol{0}_{1\times2} & \boldsymbol{0}_{1\times2} & \boldsymbol{0}_{1\times3} & \boldsymbol{0}_{1\times2} & \boldsymbol{0}_{1\times2} & 0 & 0 \\ \boldsymbol{0}_{1\times3} & \boldsymbol{0}_{1\times2} & \boldsymbol{0}_{1\times2} & \boldsymbol{0}_{1\times3} & \boldsymbol{0}_{1\times2} & \boldsymbol{0}_{1\times2} & 0 & 0 \end{bmatrix},$$

TABLE 1. The descriptions of three field tests.

Field Test number	Static stage time	Maneuvering stage time	Total distance	Maximum speed
Trajectory 1	305s	295s	2677.52m	17.02 m/s
Trajectory 2	305s	295s	2343.08m	15.65 m/s
Trajectory 3	305s	295s	3391.93m	18.21 m/s

TABLE 2. The descriptions of four in-motion alignment schemes.

Scheme number	Alignment method	Algorithm organization	Alignment result parameters
Scheme 1	IOBCA	The specific algorithm is presented in Section III in this paper. The algorithm execution begins at 300s and ends at 600s, which includes the first 5s static segment and subsequent 295s maneuvering segment.	Attitude&velocity&position
Scheme 2	OBCA	The specific algorithm is presented in [12]. The algorithm execution period is the same with Scheme 1.	Attitude&velocity
Scheme 3	IOBCA&BSFA	The specific algorithm is presented in Section III and Section IV in this paper. The algorithm execution period is the same with Scheme 1. In the BSFA, the segment from 300s to 0s denotes as backward process, and the segment from 0s to 300s denotes as forward process. And the initial parameters of backward Kalman filter and forward Kalman filter are set as follows: (1) Backward Kalman filter: $\boldsymbol{X}_0 = \mathbf{0}_{16\times1}$, $\boldsymbol{R}_k = diag\ (5/R_e\text{rad}\ \ 5/R_e\text{rad})^2$, $\boldsymbol{Q}_k = diag\ (0.01^\circ/\text{h}\ \ 0.01^\circ/\text{h}\ \ 0.01^\circ/\text{h}\ \ 100\mu\text{g}\ \ 100\mu\text{g}\ \ \mathbf{0}_{1\times11})^2$, $\boldsymbol{P}_0 = diag\ (10'\ \ 10'\ \ 5^\circ\ \ 0.1\text{m/s}\ \ 0.1\text{m/s}\ \ 20/R_e\text{rad}\ \ 20/R_e\text{rad}\ \ 0.01^\circ/\text{h}\ \ 0.01^\circ/\text{h}\ \ 0.01^\circ/\text{h}\ \ 100\mu\text{g}\ \ 100\mu\text{g}\ \ 20/R_e\text{rad}\ \ 20/R_e\text{rad}\ \ 30'\ \ 0.08)^2$ (2) Forward Kalman filter: All the forward Kalman filter parameters are initialized with the parameters provided by backward Kalman filter at the end of backward process.	Attitude&velocity&position
Scheme 4	Tradition alignment	The similar algorithm is presented in [28], while the Kalman filter model is same as Scheme 3 for the better comparison. The algorithm execution begins at 180s and ends at 600s, which includes the first 120s static coarse alignment and subsequent 300s in-motion fine alignment.	Attitude&velocity&position

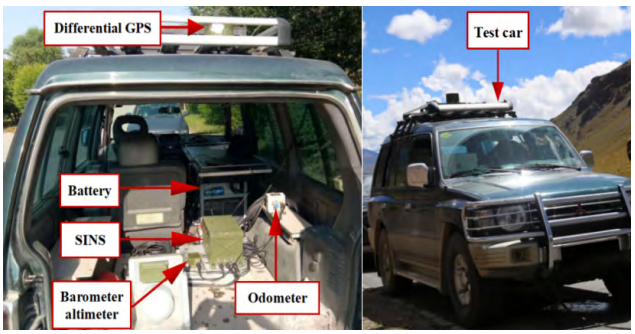

FIGURE 3. Experiment platform and equipments.

V. CAR-MOUNTED FIELD TEST

A. EXPERIMENTAL SETUP AND DESCRIPTION

The car-mounted experimental data was collected to evaluate the performance of proposed in-motion alignment method. The experimental platform is composed of the navigation-grade ring laser SINS, OD, barometric altimeter, Differential GPS (DGPS) and test car, as shown in Fig. 3. The navigation-grade ring laser SINS consists of three Ring Laser Gyroscopes (RLG) with a drift rate of $0.01^\circ/\text{h}$ (1σ) and three quartz accelerometers with a bias of 100 μg (1σ). The update rate of body angular rate, specific force and mileage increment, which are measured by RLG, accelerometer and OD, respectively, are equally 100 Hz. The scale factor and installations of OD are accurately calibrated before the field test. The DGPS provides the position with an accuracy of 3cm (1σ) at 1Hz, and lever arm of the DGPS has been estimated and compensated.

Three car-mounted field tests were carried out to verify the proposed method sufficiently, and the corresponding trajectories are shown in Fig. 4. The descriptions of three field tests are summarized in Table 1. We can see that the car firstly stayed static for about 305s and then ran in maneuvering environments for about 295s during each field test, and the corresponding total distance and maximum speed are different. It should be noted that the car was moving in open area so that DGPS was able to work normally all the time. In this respect, the SINS/DGPS integrated navigation system introduced in [26] can provide consecutive attitude, velocity and position reference. That is to say, the attitude, velocity and position reference can be provided by 300s stationary-base alignment [27] and 300s SINS/DGPS integrated navigation system.

B. COMPARISONS OF DIFFERENT IN-MOTION ALIGNMENT ALGORITHMS

For comparison, four in-motion alignment schemes are carried out using car-mounted data. The descriptions including Scheme number, alignment method, algorithm organization and alignment result parameters are summarized in Table 2.

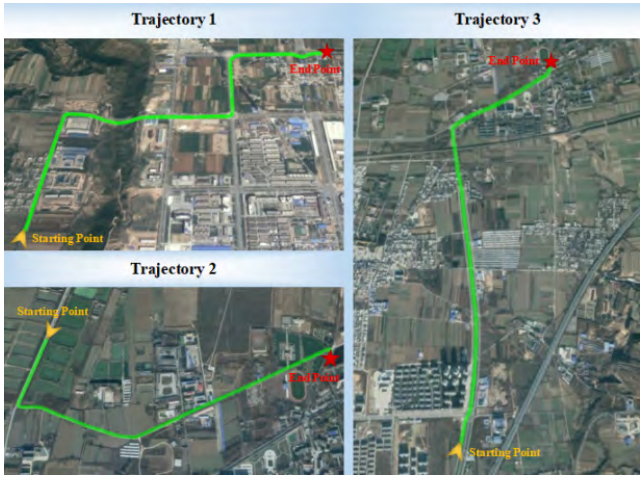

FIGURE 4. Car-mounted field test trajectories.

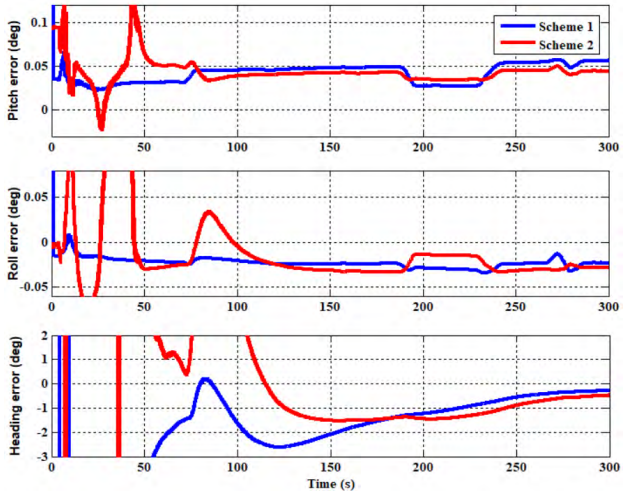

FIGURE 5. Attitude errors estimated by Scheme 1 and Scheme 2 in trajectory 1.

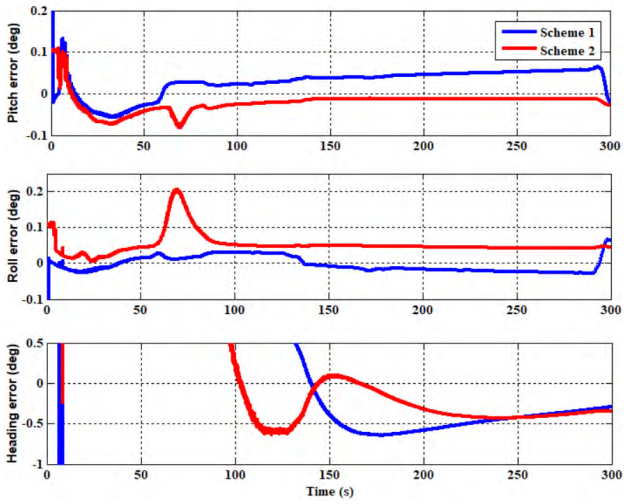

FIGURE 6. Attitude errors estimated by Scheme 1 and Scheme 2 in trajectory 2.

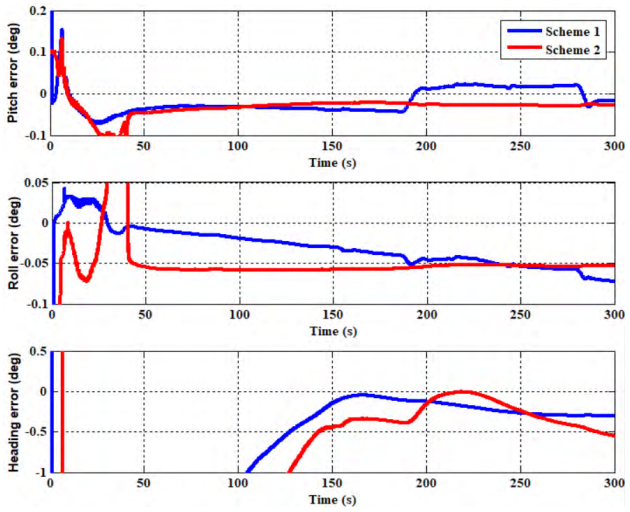

FIGURE 7. Attitude errors estimated by Scheme 1 and Scheme 2 in trajectory 3.

It should be noted that the four schemes can be executed without the aid of GPS. And all the schemes are coded with MATLAB on a computer with Intel Core i7-6700HQ CPU, 8G memory and the Windows 10 operating system.

First, Scheme 1 is implemented to provide the initial navigation parameters for BSFA. In the meantime, Scheme 2 is carried out utilizing the same test segment data to make comparison. The attitude comparison curves including pitch error, roll error and heading error between Scheme 1 and Scheme 2 are presented in Figs. 5–7. The horizontal velocity error curves including east velocity and north velocity estimated by Scheme 1 and Scheme 2 are shown in Fig. 8. The horizontal position error curves estimated by Scheme 1 are shown in Fig. 9. Meanwhile, the final attitude errors and the root mean-square (RMS) of horizontal velocity errors estimated by Scheme 1 and Scheme 2, as well as the final horizontal position errors estimated by Scheme 1 are summarized in Table 3.

According to the attitude results of three trajectories estimated by Scheme 1 and Scheme 2, we can see that both two schemes have showed comparable level in horizontal attitude estimation. While the heading estimated by Scheme 1 has superiority over Scheme 2. The reason is that the gravity deflexion error projection in inertial frame caused by the displacement of carrier is diminished in Scheme 1, which contributes to better estimations of the heading. In contrast, since Scheme 2 cannot derive position, the position should be approximated by the known initial binding position thus degrading the precision of heading estimation. As for the horizontal velocity results of Scheme 1 and Scheme 2, the root mean-square (RMS) results of horizontal velocity error estimated by Scheme 1 is all smaller than Scheme 2. The reason is that the attitude estimation fluctuation of Scheme 1 is smaller than Scheme 2 at the beginning of coarse alignment. With the

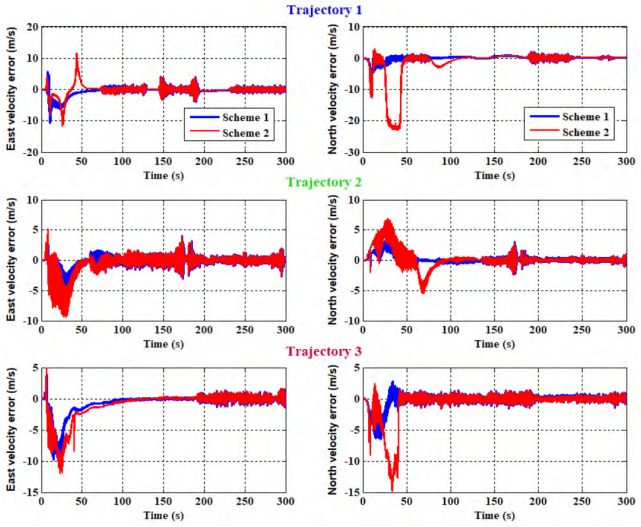

FIGURE 8. Horizontal velocity errors estimated by Scheme 1 and Scheme 2 in three trajectories.

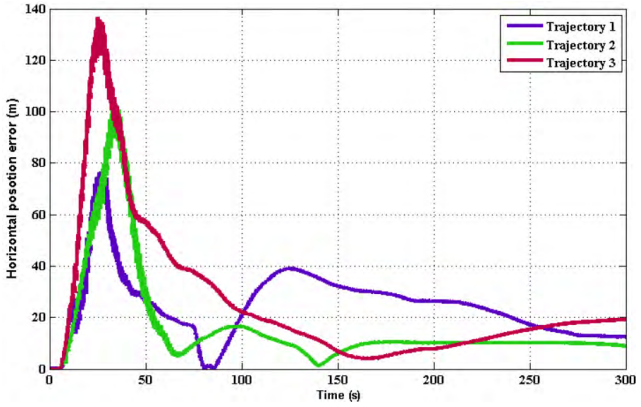

FIGURE 9. Horizontal position errors estimated by Scheme 1 in three trajectories.

improvements of attitude estimations, the horizontal velocity errors of two schemes have both decreased and the precision of velocity is mainly determined by the OD measurements. As for the horizontal position results of Scheme 1 and Scheme 2, as previously mentioned, only Scheme 1 is able to achieve the position with rational precision. And the rational position provided for BSFA is vitally important to overcome the filter divergence caused by measurement mutation when the initial binding position is introduced at the start of forward process. Therefore, the final coarse alignment results including attitude, velocity and position estimated by Scheme 1 are considered to better guarantee the smooth implementation of BSFA.

Then, to further improve the precision of in-motion alignment, the BSFA initialized with the coarse alignment results provided by Scheme 1 is carried out. And Scheme 4 including 120s stationary-base coarse alignment and 300s in-motion fine alignment is executed for comparison. For the convenience of comparison, the delay time t_D which is very short in

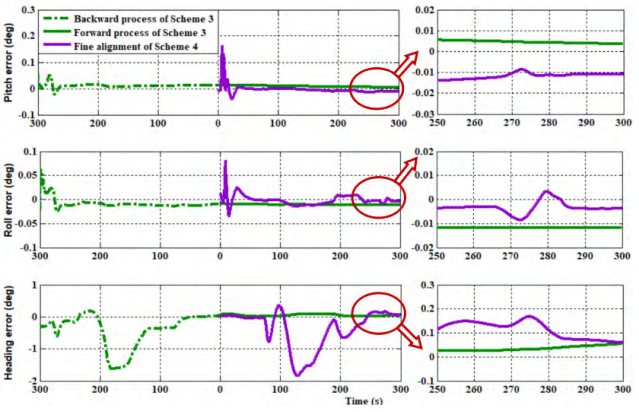

FIGURE 10. Attitude errors estimated by Scheme 3 and Scheme 4 in trajectory 1.

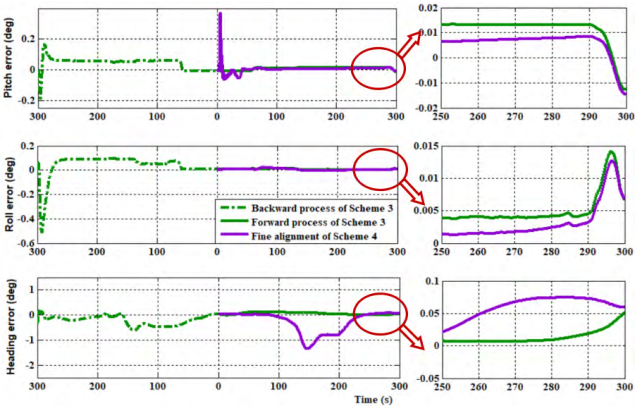

FIGURE 11. Attitude errors estimated by Scheme 3 and Scheme 4 in trajectory 2.

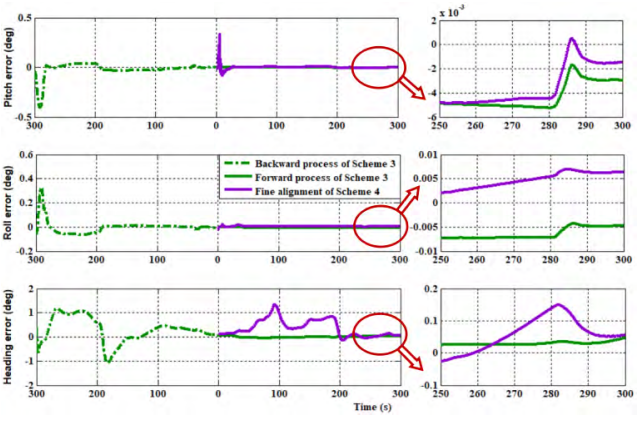

FIGURE 12. Attitude errors estimated by Scheme 3 and Scheme 4 in trajectory 3.

Scheme 3 is omitted. The attitude comparison curves including pitch error, roll error and heading error during in-motion fine alignment process between Scheme 3 and Scheme 4 in three trajectories are presented in Figs. 10–12. The horizontal velocity error curves including east velocity and north velocity estimated by the forward process of Scheme 3 and the

TABLE 3. The alignment results from different in-motion alignment methods.

Trajectory number	In-motion alignment methods		Final pitch error	Final roll error	Final heading error	Horizontal velocity error (RMS)	Final horizontal position error	Time cost
Trajectory 1	IOBCA	Scheme 1	0.0563°	-0.0231°	-0.2844°	1.767m/s	12.55m (4.69‰D)	300s
	OBCA	Scheme 2	0.0445°	-0.0283°	-0.3760°	5.425m/s	—	300s
	IOBCA & BSFA	Scheme 3	0.0036°	-0.0117°	0.0540°	0.039m/s	1.01m (0.38‰D)	300s
	Tradition alignment	Scheme 4	-0.0110°	-0.0038°	0.0585°	0.044m/s	1.17m (0.44‰D)	420s
Trajectory 2	IOBCA	Scheme 1	-0.0186°	0.0641°	-0.2891°	1.209m/s	8.81m (3.76‰D)	300s
	OBCA	Scheme 2	-0.0269°	0.0448°	-0.3453°	2.325m/s	—	300s
	IOBCA & BSFA	Scheme 3	-0.0127°	0.0067°	0.0510°	0.035m/s	1.62m (0.69‰D)	300s
	Tradition alignment	Scheme 4	-0.0146°	0.0069°	0.0595°	0.042m/s	2.01m (0.86‰D)	420s
Trajectory 3	IOBCA	Scheme 1	-0.0170°	-0.0722°	-0.3046°	2.200m/s	19.21m (5.66‰D)	300s
	OBCA	Scheme 2	-0.0271°	-0.0536°	-0.5466°	3.616m/s	—	300s
	IOBCA & BSFA	Scheme 3	-0.0030°	-0.0047°	0.0476°	0.037m/s	2.63m (0.78‰D)	300s
	Tradition alignment	Scheme 4	-0.0015°	0.0064°	0.0563°	0.040m/s	3.05m (0.90‰D)	420s

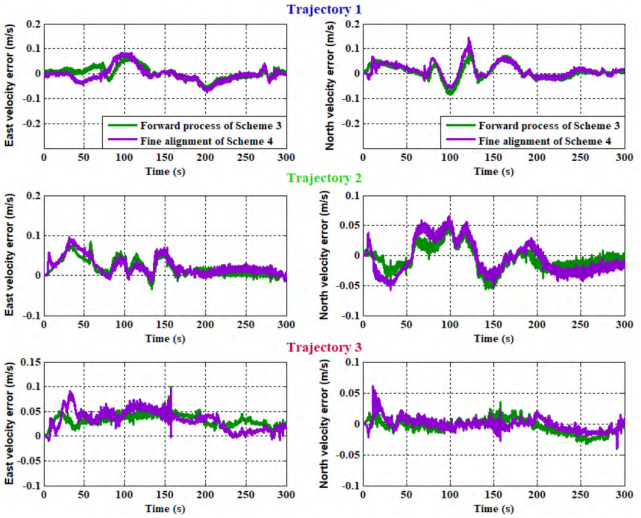

FIGURE 13. Horizontal velocity errors estimated by Scheme 3 and Scheme 4 in three trajectories.

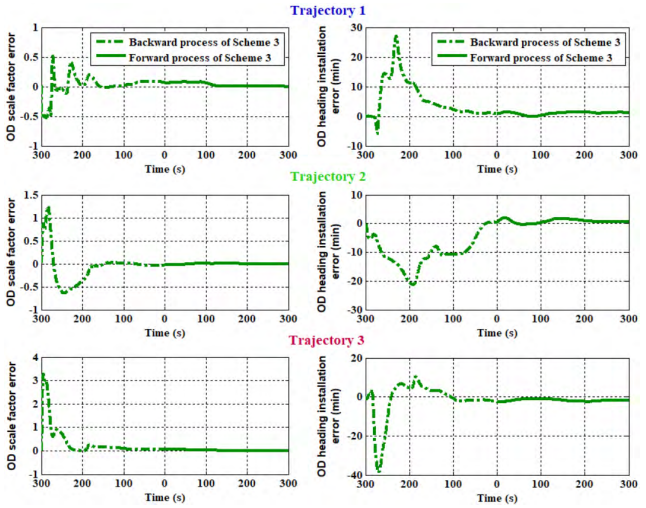

FIGURE 14. OD scale factor errors and heading installation errors estimated by Scheme 3 in three trajectories.

fine alignment of Scheme 4 are shown in Fig. 13. The OD errors including δK_D and $\delta\alpha_\varphi$ estimated by Scheme 3 in three trajectories are shown in Fig. 14. The δK_D estimation results in three trajectories are -0.00084, -0.00801 and -0.0039, respectively. The $\delta\alpha_\varphi$ estimation results in three trajectories are $1.198'$, $0.581'$ and $-1.759'$, respectively. The horizontal position error curves estimated by Scheme 3 and Scheme 4 in three trajectories are shown in Figs. 15–17. In the Scheme 3, the initial binding position is introduced to compensate the position estimation error of at the start of forward process, the position compensations in three trajectories are 0.73m, 0.77m and 0.64m, respectively. Meanwhile, the final attitude errors, the RMS of horizontal velocity errors and the final horizontal position errors estimated by Scheme 3 and Scheme 4 are summarized in Table 3.

According to the attitude results of Scheme 3 and Scheme 4, there are slight changes existing in pitch and roll error during the 290s to 300s of trajectory 2 and the 280s to 290s of trajectory 3. The reason is that the car had made a turn during the aforementioned segment, and turning motion will change attitude, which contributes to the separation of horizontal accelerometer biases. In this respect, the error estimations of pitch and roll will change slightly. Despite the existence of slight changes in pitch and roll errors, both Scheme 3 and Scheme 4 have achieved higher precision in attitude than Scheme 1 and Scheme 2. The performances of the horizontal attitudes estimated by Scheme 3 and Scheme 4 are comparable, while the heading angles in three trajectories estimated by Scheme 3 are better than Scheme 4. The main reason is that the alignment time of Scheme 3 has

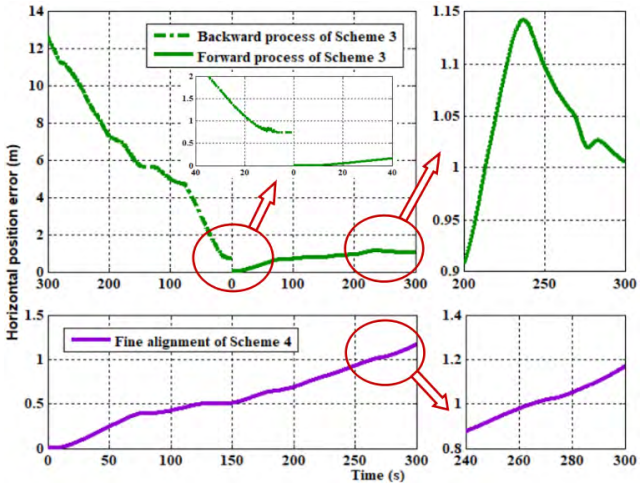

FIGURE 15. Horizontal position errors estimated by Scheme 3 and Scheme 4 in trajectory 1.

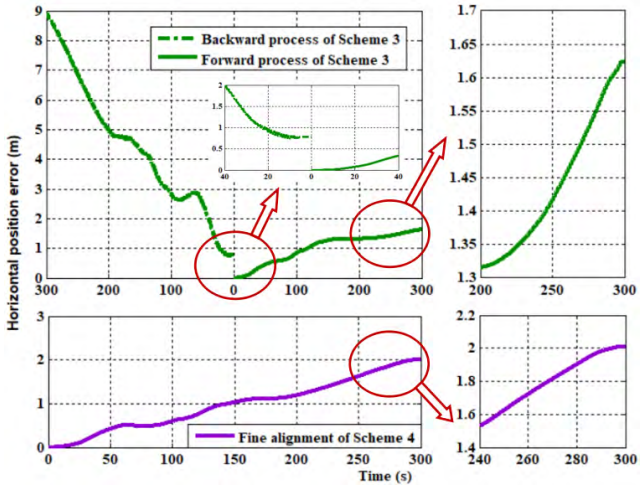

FIGURE 16. Horizontal position errors estimated by Scheme 3 and Scheme 4 in trajectory 2.

been equivalently lengthened due to the backtracking scheme, which contributes to better estimations of heading angle. As for the comparison results of velocity and position, the performances of Scheme 3 and Scheme 4 are comparable, which are better than that of Scheme 1 and Scheme 2. The first reason is that Kalman filter is an well-known method to drop the influence of measurement noise, which helps to smooth the velocity and position estimations. The second reason is that the OD heading installation error and OD scale factor error are included in SINS/OD model, which are observable during the accelerating and decelerating process of the car, thus contributing to the velocity and position estimations. Furthermore, similar to Scheme 1 and Scheme 2, Scheme 3 has no use for long-term stationary preparation at start time, thus the time cost of Scheme 3 is lower than Scheme 4. That is to say, Scheme 3 also has the significant advantage of rapid-reaction capability. Consequently, the proposed method

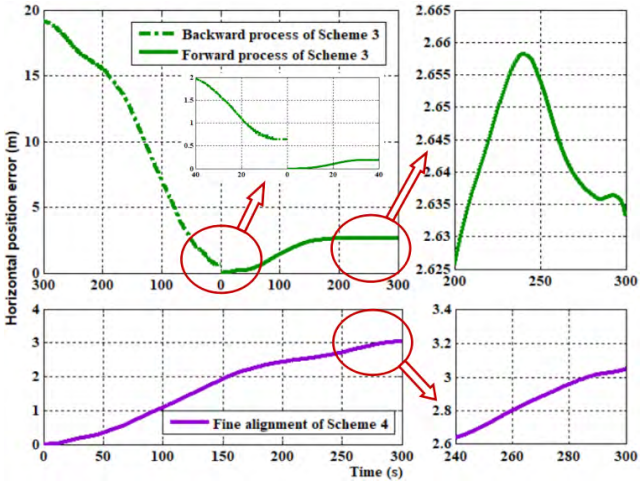

FIGURE 17. Horizontal position errors estimated by Scheme 3 and Scheme 4 in trajectory 3.

can autonomously and simultaneously achieve better attitude and position alignment results within short time than other compared schemes.

VI. CONCLUSION

In this paper, the authors focused on improving the performances of attitude and position alignment for SINS/OD under maneuvering conditions, only when the initial information including initial binding position and zero velocity are known. First, IOBCA which aims at diminishing the gravity deflexion error is executed to obtain the attitude, velocity and position with rational precision. Second, initialized with the final alignment results provided by IOBCA, BSFA combined with Kalman filter is carried out. In BSFA, the in-motion alignment time has been equivalently lengthened and the known initial information has been utilized sufficiently to suppress the velocity and position errors. Due to the rational alignment results provided by IOBCA, Kalman filter will overcome the divergency caused by position measurement mutation at the start of forward process. Moreover, the OD errors have been compensated to contribute better estimation results. The experimental results illustrated that the proposed method can not only autonomously improve the precision of attitude within short time, but also simultaneously achieve the position with high precision.

It should be noted that the investigated method is only suitable for navigation-grade SINS combined with high-precision OD. When it comes to the low-cost SINS or the low-resolution OD, the performances of the investigated method will be severely degraded. Because the inherent errors existing in low-cost sensors will lead to a weak IOBCA performance. Even if the IOBCA alignment results satisfy the linearization requirements of subsequent BSFA, the increased sensor observation noises will also cause the nonlinearization of SINS/OD model. As a result, the ideal attitude and position precision cannot be obtained. Therefore, future work is needed to extend the application of the investigated method

and make it more accessible to the low-cost SINS with low-resolution OD.

REFERENCES

[1] D. Titterton and J. Weston, *Strapdown Inertial Navigation Technology*, 2nd ed. London, U.K.: IET, 2004, pp. 3–8.
[2] Y. G. Tang, Y. Wu, M. Wu, W. Wu, X. Hu, and L. Shen, "INS/GPS integration: Global observability analysis," *IEEE Trans. Veh. Technol.*, vol. 58, no. 3, pp. 1129–1142, Mar. 2009.
[3] Y. Huang and Y. Zhang, "A new process uncertainty robust Student's t based Kalman filter for SINS/GPS integration," *IEEE Access*, vol. 5, pp. 14391–14404, 2017.
[4] Y. Wu, C. Goodall, and N. El-Sheimy, "Self-calibration for IMU/odometer land navigation: Simulation and test results," in *Proc. Int. Tech. Meeting Inst. Navigat.*, San Diego, CA, USA, 2010, pp. 839–849.
[5] Z. Li, J. Wang, B. Li, J. Gao, and X. Tan, "GPS/INS/Odometer integrated system using fuzzy neural network for land vehicle navigation applications," *J. Navigat.*, vol. 67, no. 6, pp. 967–983, Nov. 2014.
[6] P. D. Groves, *Principles of GNSS, Inertial, and Multisensor Integrated Navigation Systems*, 2nd ed. Norwood, MA, USA: Artech House, 2013.
[7] F. Jiancheng and Y. Sheng, "Study on innovation adaptive EKF for in-flight alignment of airborne POS," *IEEE Trans. Instrum. Meas.*, vol. 60, no. 4, pp. 1378–1388, Apr. 2011.
[8] H. Yu, H. Zhu, D. Gao, M. Yu, and W. Wu, "A stationary north-finding scheme for an azimuth rotational IMU utilizing a linear state equality constraint," *Sensors*, vol. 15, no. 2, pp. 4368–4387, Feb. 2015.
[9] D. Gu, N. El-Sheimy, T. Hassan, and Z. Syed, "Coarse alignment for marine SINS using gravity in the inertial frame as a reference," in *Proc. IEEE/ION PLANS*, Monterey, CA, USA, May 2008, pp. 961–965.
[10] Y. Y. Qin, G. M. Yan, D. Q. Gu, and J. B. Zheng, "A clever way of SINS coarse alignment despite rocking ship," *J. Northwestern Polytech. Univ.*, vol. 23, no. 5, pp. 681–684, Oct. 2005.
[11] M. Wu, Y. Wu, X. Hu, and D. Hu, "Optimization-based alignment for inertial navigation systems: Theory and algorithm," *Aerosp. Sci. Technol.*, vol. 15, no. 1, pp. 1–17, Jan./Feb. 2011.
[12] D. Yuan, X. Ma, Y. Liu, C. Hao, and Y. Zhu, "Dynamic initial coarse alignment of SINS for AUV using the velocity loci and pressure sensor," *IET Sci., Meas. Technol.*, vol. 10, no. 8, pp. 926–933, Nov. 2016.
[13] L. Chang, H. He, and F. Qin, "In-motion initial alignment for odometer-aided strapdown inertial navigation system based on attitude estimation," *IEEE Sensors J.*, vol. 17, no. 3, pp. 766–773, Feb. 2017.
[14] Y. Huang, Y. Zhang, and X. Wang, "Kalman-filtering-based in-motion coarse alignment for odometer-aided SINS," *IEEE Trans. Instrum. Meas.*, vol. 66, no. 12, pp. 3364–3377, Dec. 2017.
[15] F. L. Markley and J. L. Crassidis, *Fundamentals of Spacecraft Attitude Determination and Control*. Portland, OR, USA: Springer, 2014.
[16] L. Chang, Y. Li, and B. Xue, "Initial alignment for a Doppler velocity log-aided strapdown inertial navigation system with limited information," *IEEE/AMSE Trans. Mechatronics*, vol. 22, no. 1, pp. 329–338, Feb. 2017.
[17] G. M. Yan, J. Weng, L. Bai, and Y. Y. Qin, "Initial in-movement alignment and position determination based on inertial reference frame," *Syst. Eng. Electron.*, vol. 33, no. 3, pp. 618–621, 2011.
[18] S. Guo, J. Xu, and H. He, "External velocity aided coarse attitude and position alignment for dynamic SINS," *IEEE Access.*, vol. 6, pp. 15099–15105, 2018.
[19] L. Chang, B. Hu, and Y. Li, "Backtracking integration for fast attitude determination-based initial alignment," *IEEE Trans. Instrum. Meas.*, vol. 64, no. 3, pp. 795–803, Mar. 2015.
[20] L. Chang, F. Qin, and A. Li, "A novel backtracking scheme for attitude determination-based initial alignment," *IEEE Trans. Autom. Sci. Eng.*, vol. 12, no. 1, pp. 384–390, Jan. 2015.
[21] W. Li, W. Wu, J. Wang, and M. Wu, "A novel backtracking navigation scheme for autonomous underwater vehicles," *Measurement*, vol. 47, pp. 496–504, Jan. 2014.
[22] W. Li, W. Wu, J. Wang, and L. Lu, "A fast SINS initial alignment scheme for underwater vehicle applications," *J. Navigat.*, vol. 66, no. 2, pp. 181–198, Mar. 2013.
[23] G. Wahba, "A least squares estimate of satellite attitude," *SIAM Rev.*, vol. 7, no. 3, pp. 385–386, 1965.
[24] Y. Gongmin, Y. Weisheng, and X. Demin, "On reverse navigation algorithm and its application to SINS gyro-compass in-movement alignment," in *Proc. 27th Chin. Control Conf.*, Kunming, China, Jul. 2008, pp. 724–729.
[25] H. Xue, X. Guo, Z. Zhou, and K. Wang, "In-motion alignment algorithm for vehicle carried SINS based on odometer aiding," *J. Navigat.*, vol. 70, no. 6, pp. 1349–1366, Nov. 2017.
[26] P. G. Savage, *Strapdown Analytics*, 2nd ed. Maple Plain, MN, USA: Strapdown Associates, 2007.
[27] F. O. Silve, E. M. Hemerly, and W. L. Filho, "On the error state selection for stationary SINS alignment and calibration Kalman filters—Part I: Estimation algorithms," *Aerosp. Sci. Technol.*, vol. 61, pp. 45–56, Feb. 2017.
[28] W. Gao, X. Zhang, G. Zhao, and Y. Ben, "A fine alignment method about Doppler-assisted SINS," in *Proc. Int. Conf. Inf. Automat.*, Harbin, China, Jun. 2010, pp. 2333–2337.

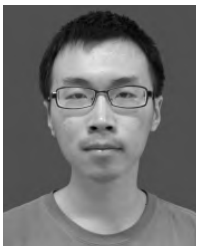

YIDING SUN received the B.E. degree in measurement and control technology and instrumentation from Harbin Engineering University, Harbin, China, in 2015. He is currently pursuing the Ph.D. degree with the School of Instrumentation and Optoelectronic Engineering, Beihang University.

His current research interests include inertial navigation and integrated navigation.

LIFEN WANG received the Ph.D. degree in precision instrumentation and mechanism from Beihang University, Beijing, China, in 2015, where she currently holds a Postdoctoral position with the School of Instrumentation and Optoelectronic Engineering.

Her current research interests include inertial navigation and integrated navigation.

QINGZHONG CAI received the Ph.D. degree in optical engineering from Beihang University, Beijing, China, in 2014, where he is currently a Research Associate with the School of Instrumentation and Optoelectronic Engineering.

His current research interests include inertial navigation and integrated navigation.

GONGLIU YANG received the Ph.D. degree in precision instrumentation and mechanism from Tsinghua University, Beijing, China, in 2004.

He is currently a Professor with the School of Instrumentation and Optoelectronic Engineering, Beihang University. His current research interests include inertial navigation and integrated navigation.

ZEYANG WEN received the B.S. degree in integrated circuit from Xidian University, Xi'an, Shaanxi, China, in 2017. He is currently pursuing the Ph.D. degree with the School of Instrumentation and Optoelectronic Engineering, Beihang University.

His research interest includes the error mitigation method of long-term independent inertial navigation.